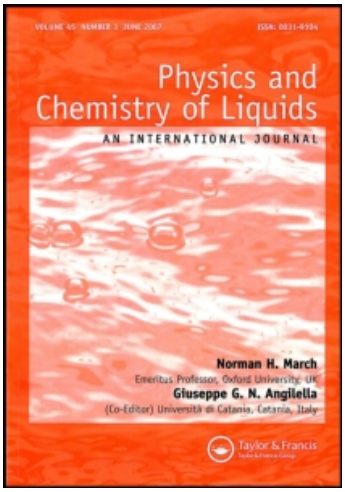

Physics and Chemistry of Liquids
Publication details, including instructions for authors and subscription information:
http://www.informaworld.com/smpp/title~content=t713646857

From molecular clusters to liquid structure in $AlCl_3$ and $FeCl_3$

E. Goat[a]; R. Ruberto[b]; G. Pastore[ab]; Z. Akdeniz[c]; MP Tosi[d]
[a] Dipartimento di Fisica Teorica dell'Università, I-34100 Trieste, Italy [b] CNR-INFM DEMOCRITOS National Simulation Center, I-34100 Trieste, Italy [c] Physics Department, Istanbul University, 34118 Vezneciler-Istanbul, Turkey [d] NEST-CNR-INFM, Scuola Normale Superiore, I-56126 Pisa, Italy

To cite this Article Goat, E. , Ruberto, R. , Pastore, G. , Akdeniz, Z. and Tosi, MP(2007) 'From molecular clusters to liquid structure in $AlCl_3$ and $FeCl_3$', Physics and Chemistry of Liquids, 45: 5, 487 — 501
To link to this Article: DOI: 10.1080/00319100701371084
URL: http://dx.doi.org/10.1080/00319100701371084

Physics and Chemistry of Liquids
Vol. 45, No. 5, October 2007, 487–501

Taylor & Francis
Taylor & Francis Group

From molecular clusters to liquid structure in $AlCl_3$ and $FeCl_3$

E. GOAT†, R. RUBERTO‡, G. PASTORE*†‡,
Z. AKDENIZ§ and M. P. TOSI¶

†Dipartimento di Fisica Teorica dell'Università,
Strada Costiera 11, I-34100 Trieste, Italy
‡CNR-INFM DEMOCRITOS National Simulation Center,
Via Beirut 2, I-34100 Trieste, Italy
§Physics Department, Istanbul University, 34118 Vezneciler-Istanbul, Turkey
¶NEST-CNR-INFM, Scuola Normale Superiore,
Piazza dei Cavalieri 7, I-56126 Pisa, Italy

(*Received 23 March 2007; in final form 29 March 2007*)

Melting of aluminum and iron trichloride is accompanied by a structural transition from sixfold to fourfold coordination of the trivalent metal ions, and a widely accepted interpretation of the structure of their melts near freezing is that they mainly consist of strongly correlated dimers formed from two edge-sharing tetrahedra. We carry out classical molecular dynamics simulations to examine how a polarizable-ion force law, determined on isolated molecular monomers and dimers in the gaseous phase of these compounds, fares in accounting for the pair structure of their liquid phase and for mean square displacements and diffusion coefficients of the two species in each melt. The model reproduces the main features of the neutron diffraction structure factor, showing peaks due to intermediate range order and to charge and density short-range order, and accounts for the experimental data at a good semi-quantitative level. We find agreement with the neutron and X-ray diffraction data on metal–halogen and Cl–Cl bond lengths in the melt, and demonstrate the high sensitivity of the results for the width of the first-neighbor shell to truncation in obtaining it by Fourier transform of the neutron-weighted structure factor in momentum space. We also report comparisons with a recent first-principles study of the structure of the $AlCl_3$ melt by the Car–Parrinello method. Finally, we demonstrate break-up of dimers into monomers upon raising the liquid temperature in the case of $AlCl_3$.

Keywords: Liquid structure from model simulations; Molten salts; Molecular liquids

1. Introduction

$AlCl_3$ and $FeCl_3$ are the only binary ionic materials whose local structure is known to drastically change its type on melting [1]. Let us first contrast their crystal structure with those of other trihalides, and specifically with those of YCl_3 and $AlBr_3$. The crystal

*Corresponding author. Email: pastore@ts.infn.it

ISSN 0031-9104 print/ISSN 1029-0451 online © 2007 Taylor & Francis
DOI: 10.1080/00319100701371084

structures of YCl_3 and $AlCl_3$ are isomorphous and are formed from slightly distorted cubic close-packed arrangements of the chlorines, inside which the metal ions occupy alternate layers of octahedral sites. Such a layer structure possessing sixfold coordination of the metal ions is also present in crystalline $FeCl_3$, except that the layer stacking is close-packed hexagonal rather than cubic. In crystalline $AlBr_3$ the packing of the bromines is also hexagonal, but the metal ions occupy tetrahedral sites such that the crystal can be viewed as formed from Al_2Br_6 dimeric units in the shape of two edge-sharing tetrahedra. A cooperative rearrangement of the metal ions in the $AlCl_3$-type crystal structure from octahedral to tetrahedral sites, accompanied by a change of the stacking from cubic to hexagonal, would effect a solid-state structural transition into the $AlBr_3$-type structure [2].

Turning to the melting behavior of these compounds, YCl_3 retains on melting a close-packed structure with approximately octahedral coordination of the metal ions [3,4]. Instead, melting of $AlCl_3$ and $FeCl_3$ is accompanied by a transition bringing the metal ions from sixfold to approximately fourfold coordination and yields liquids which have been described as mainly made of Al_2Cl_6 or Fe_2Cl_6 molecular dimers [5,6]. The dimer-based structure of the $AlBr_3$ crystal is preserved on melting [7]. These different melting mechanisms are reflected in the values of the melting parameters: in the sequence YCl_3, $AlCl_3$, $FeCl_3$ and $AlBr_3$, the relative volume change $\Delta V/V_{liq}$ is 0.0045, 0.47, 0.39 and 0.18, and the entropy change ΔS equals 7.56, 18.1, 17.8 and 7.3 e.u. [8]. The view that melting of $AlCl_3$ yields a molecular liquid of correlated Al_2Cl_6 dimers was first proposed on the basis of X-ray diffraction data by Harris *et al.* [9] and is also consistent with the Raman scattering spectra of trihalide melts [10]. Measurements of the total neutron diffraction pattern of molten $AlCl_3$ [11] have confirmed the fourfold coordination of the metal ions, whereas a slightly lower value of the average Fe–Cl coordination number has been reported from neutron diffraction experiments on molten $FeCl_3$ [6,12]. Some residual structural differences between the $AlCl_3$ and $FeCl_3$ melts are also implied by the values of their ionic conductivity σ: in $\Omega^{-1}\,cm^{-1}$, the measured values in the melt near freezing [13] are $\sigma = 5 \times 10^{-7}$ in $AlCl_3$ and 0.04 in $FeCl_3$, to be compared with $\sigma = 0.39$ in molten YCl_3 and with $\sigma = 1 \times 10^{-8}$ in molten $AlBr_3$. A partial ionization equilibrium resulting from some chlorine-ion transfer between dimers has been proposed for molten $FeCl_3$ near freezing [14].

The similarity of $AlCl_3$ and $FeCl_3$ in melting behavior and in local liquid structure extends to the structure of their vapors. The Al_2Cl_6 and Fe_2Cl_6 molecular dimers are the main constituents of the low-temperature gas, and indeed the two dimers coexist with $AlFeCl_6$ molecules in gaseous mixtures [15]. Raman scattering experiments on gaseous $AlCl_3$ indicate a transition from a mixture of dimers and monomers at the sublimation point to a purely monomeric gas at 900°C [16], and electron diffraction experiments yield a fraction of about 29% dimers in $AlCl_3$ gas at 400°C [17].

We present in this work the results of classical molecular dynamics runs focusing on how well an ionic interaction law determined from properties of the isolated molecular clusters in the gas fares in regard to the observed pair structure from the neutron diffraction experiments on the liquid phase of $AlCl_3$ and $FeCl_3$ near freezing [11,12]. The interionic force law is taken from the work of Akdeniz *et al.* [18], who carried out a systematic study of the binding and the vibrational frequencies of monomeric and dimeric units of Al, Fe and Ga chlorides, bromides and iodides. They also considered ionized states formed by stripping or adding a halogen ion, in addition to neutral molecular states. Previous computer simulation studies of the liquid structure

of trihalides have been reported by Abramo and Caccamo [19] and by Madden and coworkers [20,21]. The structure of the $AlCl_3$ melt has very recently been studied in first-principles simulations using the Car–Parrinello method [22].

The ionic interactions in our approach are constructed from Born–Mayer-type pair potentials supplemented by shell-model dipoles located on the halogens. The inclusion of ion-core polarization resulting on the halogens from electrical induction as well as from overlap deformability is indeed crucial to quantitatively emulate chemical bonding in binary ionic systems. We refer specifically in this connection to the work of Karaman *et al.* on the NaCl monomer [23], showing excellent quantitative agreement of this model with measured molecular properties at equilibrium and with the potential energy curve of the molecule as determined in quantum-chemical configuration-interaction calculations over a wide range of internuclear distances. Most importantly, the present approach to trihalide melts not only allows for ionization processes leading to ionic conduction in standard thermodynamic conditions, but is also suitable for computer simulation studies of these melts in far-removed thermodynamic states in which large increases in temperature and pressure have induced breakage of dimers and ultimately led to full ionization. We illustrate this potentiality below by following the breakage of dimers into monomers with increasing temperature of the $AlCl_3$ liquid. This is in contrast with the common approach to molecular liquids, which is based on force laws acting between unbreakable molecular units.

The plan of the article is briefly as follows. The essential aspects of the model are recalled in section 2, which also gives some details on the simulation method using microcanonical molecular dynamics. Section 3 reports our main results for the structure and the single-particle motions in the $AlCl_3$ and $FeCl_3$ melts. We also report in this section, comparisons with the structural results obtained for the $AlCl_3$ melt by the Car–Parrinello method [22] and results for the temperature dependence of the pair structure of this liquid. Comparisons with the classical simulation results given by Hutchinson *et al.* [20], who used a model constructed from an earlier analysis of molecular data by Pastore *et al.* [24] with some adjustments to data from neutron diffraction on the melt, have been reported elsewhere [25]. The article ends with a summary and some discussion of future perspectives in section 4.

2. Interionic force law and simulation procedure

We write the potential energy $U(\{\mathbf{r}_{ij}\},\{\mathbf{p}_i\})$ of the liquid simulation sample, which depends on all interionic bond vectors $\mathbf{r}_{ij}$ and all electronic dipoles $\mathbf{p}_i$ carried by the halogens, as

$$U(\{\mathbf{r}_{ij}\},\{\mathbf{p}_i\}) = \sum_{i<j}\left[\frac{z_i z_j e^2}{r_{ij}} + \Phi_{ij}(r_{ij}) - \frac{C_i C_j}{r_{ij}^6}\right] + U_{\mathrm{pol}}^{\mathrm{cl}}(\{\mathbf{r}_{ij}\},\{\mathbf{p}_i\}) + U_{\mathrm{shell}}(\{\mathbf{r}_{ij}\},\{\mathbf{p}_i\}). \quad (1)$$

The sum in equation (1) includes (i) the Coulomb energy of the ionic point charges having nominal valences z_i, (ii) the overlap repulsive energy as described by the Busing form [26]

$$\Phi_{ij}(r) = f(\rho_i + \rho_j)\exp\left[\frac{(R_i + R_j - r)}{(\rho_i + \rho_j)}\right], \quad (2)$$

in terms of transferable radii R_i and stiffness parameters ρ_i, and (iii) the van der Waals energy of the halogens. The electronic polarization of the halogens is allowed through both the classical polarization energy $U_{\mathrm{pol}}^{\mathrm{cl}}$ and the shell deformation energy U_{shell}, the latter being patterned after the shell model used in the lattice dynamics of ionic and semiconducting crystals; see e.g. [27]. Explicit expressions for these energy terms can be found in [28]. It was also shown there that the results for bond lengths in isolated dimers are essentially unchanged when the nominal valences are replaced by effective valences, provided that use is made of the equilibrium condition in determining the overlap repulsive parameters.

Minimization of equation (1) with respect to the dipoles in a given spatial configuration of the ions yields the dipole $\mathbf{p}_h$ on the h-th halogen as the sum of a classical point-ion term proportional to the local electric field and of a counteracting dipole due to the overlap of the valence electron shell of the halogen with the neighboring metal ions,

$$\mathbf{p}_h = \alpha_h \mathbf{E}_h(\{\mathbf{r}_{ij}\},\{\mathbf{p}_i\}) + \alpha_s \sum_{i_j} \hat{\mathbf{r}}_{ih} \left| \frac{\mathrm{d}\Phi_{ih}(r_{ih})}{\mathrm{d}r_{ih}} \right|. \tag{3}$$

Here, $\mathbf{E}_h$ is the self-consistent electric field on the halogen, α_h and α_s are its electrical and short-range polarizabilities, and the sum is restricted to run over its first-neighbor metal ions. As already noted, we have taken the values of the various force law parameters from the analysis of isolated molecular structures given in [18].

With the potential energy of the ionic assembly written as a function of the bond vectors and of the dipoles on the halogens, we perform standard microcanonical molecular dynamics calculations using Beeman's algorithm [29]. Our molecular dynamics code implements a full calculation of Ewald sums for the long-range (charge–charge, charge–dipole, and dipole–dipole) interactions, allowing full control on the accuracy of the evaluation of energy and forces. The linear system of equations (3) for the dipole moments on the halogens is numerically solved at each time step: this direct strategy is quite inefficient, due to the dominant computational cost of the evaluation of the linear system coefficients in reciprocal space. However, we have ascertained that a system of 256 ions is already sufficient to yield very reliable results for the structural properties of the liquid in the thermodynamic states of present interest, and still allows us to carry out very long simulations on a personal computer. We have shown elsewhere [25] that this sample size yields results for liquid structure that are indistinguishable in practice from those obtained on smaller samples of 108 ions.

The simulation protocol is the same for $AlCl_3$ and $FeCl_3$. We initialize the system with the ions on a face-centered cubic lattice at the experimental density inside a cubic box with periodic boundary conditions and optimize the ionic positions by a sequence of 10^4 steepest descent steps. After melting and equilibrating the system at 3000 K, we cool it to the temperature of the neutron diffraction experiments and equilibrate it for 48 ps. The statistics is then collected by sampling 6000 configurations in a microcanonical run over an interval of 48 ps. A time step of 2 fs ensures excellent conservation of the energy in connection with Beeman's algorithm.

The main output of the calculation are the partial pair distribution functions (pdf) $g_{ij}(r)$, with each suffix denoting an ionic species, and the partial structure factors $S_{ij}(k)$. The former are obtained from direct counting of interionic distances in $\mathbf{r}$-space and the latter are determined by a direct method using the correlations between partial ionic

density fluctuations of wave vectors **k** and $-\mathbf{k}$. Comparisons with the structure factors obtained from the Fourier transform of $g_{ij}(r)$ have been shown elsewhere [25]. The self-diffusion coefficients of the two ionic species are obtained from their mean square displacements (msd) through the Einstein relation.

3. Results and discussion

3.1. *Total neutron structure factor and partial structure factors*

Figure 1 reports our results for the neutron-weighted structure factor $S(k)$ of the $AlCl_3$ and $FeCl_3$ melts near freezing at the experimental density ρ. $S(k)$ is defined as $S(k) = \sum_{i,j} w_{ij}[S_{ij}^{(FZ)}(k) - 1]$, where $w_{ij} = c_i c_j b_i b_j$, c_i are the concentrations of each species, b_i are the normalized neutron scattering lengths, and $S_{ij}^{(FZ)}(k)$ are the Faber–Ziman partial structure factors, defined as $S_{ij}^{(FZ)}(k) = N^{-1}\langle \delta\rho_i(\mathbf{k})\delta\rho_j(-\mathbf{k})\rangle$ with N the total number of ions and $\delta\rho_i(\mathbf{k})$ the density fluctuation of given wave vector **k** for each species. In figure 1, we also report the observed neutron diffraction patterns for the two melts [11,12]. Simulation results for the Ashcroft–Langreth partial structure factors $S_{ij}(k)$ of the $FeCl_3$ melt are shown in figure 2. The partial structure factors of the $AlCl_3$ melt have been reported elsewhere [25] and show entirely similar features to those illustrated in figure 2.

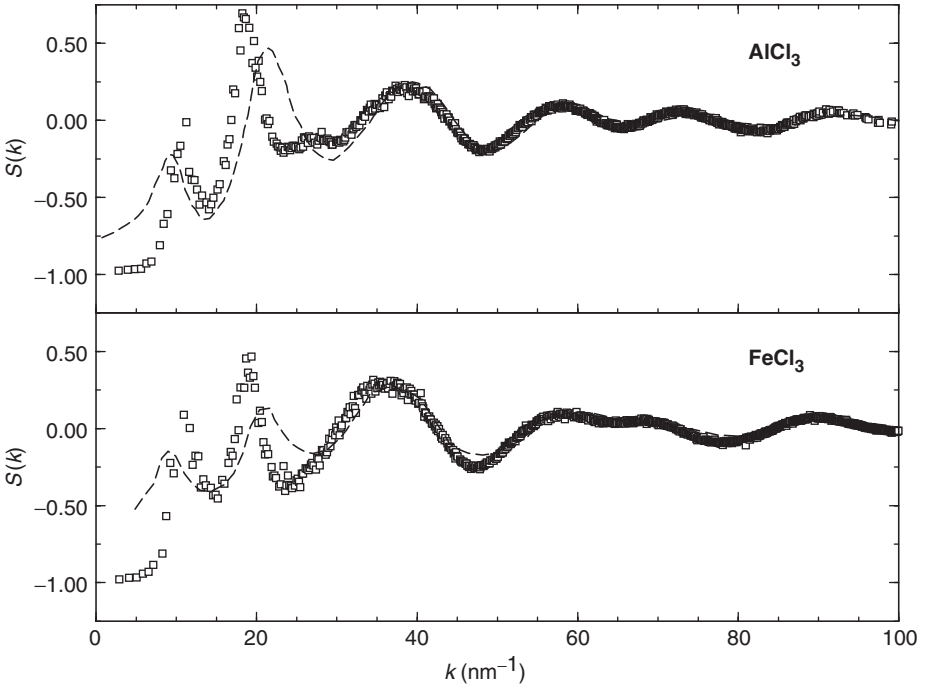

Figure 1. The squares show the neutron-weighted structure factor $S(k)$ for models of molten $AlCl_3$ at $T = 473\,K$ and $\rho = 1.27\,g\,cm^{-3}$ (top) and for molten $FeCl_3$ at $T = 600\,K$ and $\rho = 1.73\,g\,cm^{-3}$ (bottom), constructed from partial structure factors as illustrated in figure 2. The dashed lines report the measured $S(k)$ from the neutron diffraction experiments of Badyal *et al.* [11] and of Price *et al.* [12].

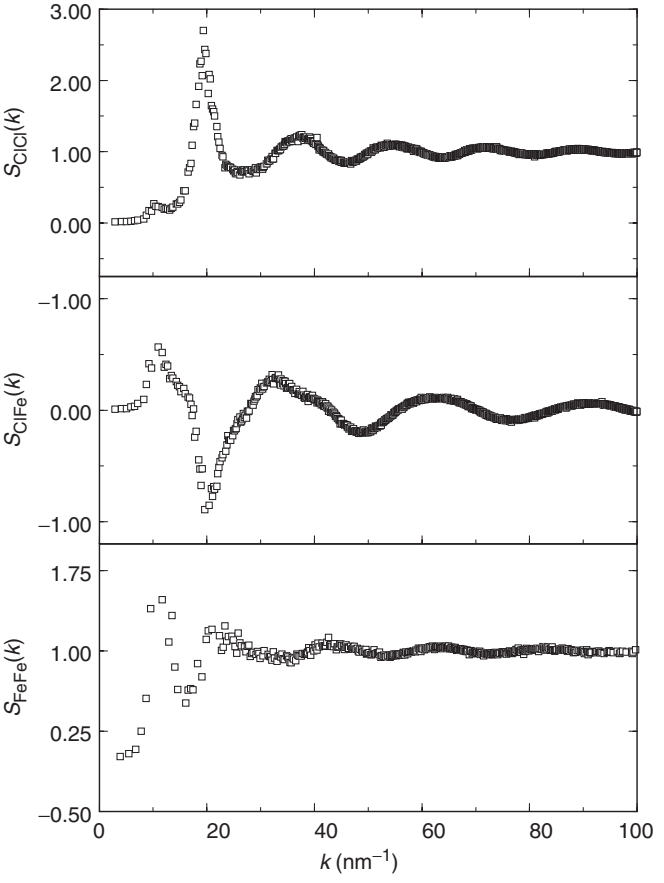

Figure 2. Ashcroft–Langreth partial structure factors $S_{ij}(k)$ of the $FeCl_3$ melt at $T = 600\,K$ and $\rho = 1.73\,g\,cm^{-3}$.

The three main peaks shown by $S(k)$ in figure 1 as k increases are due to intermediate range order and to charge and density short-range order. In fact, there is also a contribution from density–density correlations to the second peak in $S(k)$. The comparison of our results with the neutron diffraction data shows some discrepancies of detail in the location and sharpness of the first two peaks, whereas there is excellent agreement in the density–density peak and in the structures further out. We take the latter result to be a confirmation of a molecular-like state of structural order. As already illustrated in [25], there is also good agreement between our results and those of Hutchinson *et al.* [20] in both the neutron-weighted and the partial structure factors: their simulation samples were considerably larger and their model was to some extent adjusted to data on melts.

It should be remarked that the Faber–Ziman coefficients entering $S(k)$ are in the ratio $w_{AlAl}/w_{ClCl} = 0.013$ for $AlCl_3$ and $w_{FeFe}/w_{ClCl} = 0.11$ for $FeCl_3$. Thus the total neutron diffraction pattern is rather insensitive to the metal–metal correlations in $FeCl_3$ and wholly so in $AlCl_3$. The preferred value of the metal–metal bond length should directly reflect the connectivity of the metal-based fourfold units, and in the experiments

on molten $FeCl_3$ [6] the neutron scattering pattern was supplemented by the X-ray scattering pattern, which is somewhat more favorable for revealing metal-metal correlations even if full charge transfer from metal atoms to halogens is assumed. Equally good fits of the neutron scattering pattern of $AlCl_3$ were obtained by reverse Monte Carlo analyses using rather different inputs for the Al–Al bond length [11]. In the simulation runs the value of the metal–metal bond length is quite sensitive to the inclusion of halogen polarization and to the details of the model used to describe it.

3.2. *Radial distribution functions*

The full lines in figure 3 report our results for the neutron-weighted pdf $G(r)$ of the models simulating liquid $AlCl_3$ and $FeCl_3$ at the same temperature and density as in the previous figures. The dotted lines report the corresponding neutron-weighted pdf obtained by Fourier inversion of the measured $S(k)$ in the neutron scattering experiments [11,12]. $G(r)$ is given by $G(r) = 1 + \sum_{i,j} w_{ij}[g_{ij}(r) - 1]$, where $g_{ij}(r)$ are the partial radial distribution functions. Notice that with this definition $G(r)$ tends asymptotically to unity and to a finite value at short distance r. The partial distribution functions of the present model for molten $AlCl_3$ are shown in figure 4, in comparison with those obtained by Kirchner *et al.* [22] in their first-principles simulations based on two different density functionals. Finally, we show in figure 5 our results for the temperature dependence of the partial pdfs in liquid $AlCl_3$ at the equilibrium density as reported by Janz [30], after extrapolating it up to 673 K from its reported range of validity ($462\,K < T < 569\,K$).

The local liquid-state order revealed by the neutron-weighted pdf in figure 3 has three distinctive features: (i) a first-neighbor peak, which is associated with the $M–Cl^T$

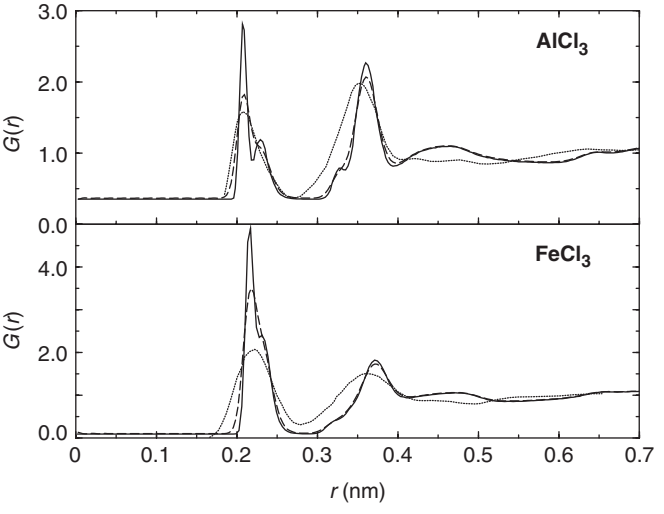

Figure 3. Neutron-weighted pdf $G(r)$ for models of molten $AlCl_3$ at $T = 473\,K$ and $\rho = 1.27\,g\,cm^{-3}$ (top) and of molten $FeCl_3$ at $T = 600\,K$ and $\rho = 1.73\,g\,cm^{-3}$ (bottom). The simulated pdf for assemblies of 256 ions is shown as solid lines, whereas the dashed lines illustrate the effect of a momentum cut-off in obtaining $G(r)$ from Fourier inversion of $S(k)$ (see text). The dotted lines report the pdf from Fourier inversion of the measured neutron-weighted diffraction pattern [11,12].

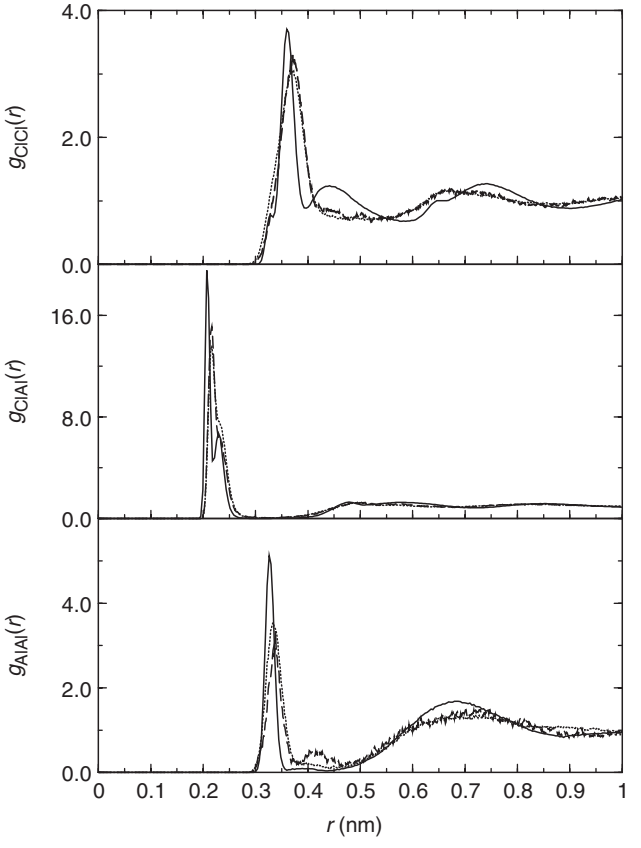

Figure 4. Partial radial distribution functions of the present model for molten $AlCl_3$ (full lines), compared with those from the *ab initio* simulation study of Kirchner *et al*. [22] with two alternative choices for the density functional (dashed and dotted lines).

bond length in the molecular dimer (with M = metal ion and Cl^T = terminal Cl) and lies at a position in very close agreement between simulation models and neutron diffraction experiments; (ii) a second main peak, which is associated with the Cl^T–Cl^T bond length in the molecular dimer and shows a discrepancy of $\approx$0.01 nm in its location between models and neutron diffraction data; and (iii) a deep trough between these two peaks, where the probability of finding ions is effectively zero in both the model and the neutron-diffraction experiment for $AlCl_3$ but finite, though very small, in the experiment on $FeCl_3$. This third feature implies, of course, that the exchange of ions between the first-neighbor shell and the rest of the liquid is effectively zero in $AlCl_3$, as is the case for a very strongly stable molecular-type first-neighbor coordination. On the other hand, the model exaggerates to some extent the stability of the first-neighbor shell in $FeCl_3$, for which the diffraction data give evidence for some chlorine exchange processes between the first-neighbor shell and the rest of the liquid. A fourth feature in the $G(r)$ of the simulation model is the small peak or shoulder on the right side of the first main peak, which is associated with the M–Cl^B bond length in the molecular dimer (with Cl^B = bonding Cl). This secondary peak is rather weaker in $FeCl_3$ than in $AlCl_3$, indicating a relatively higher proportion of monomers

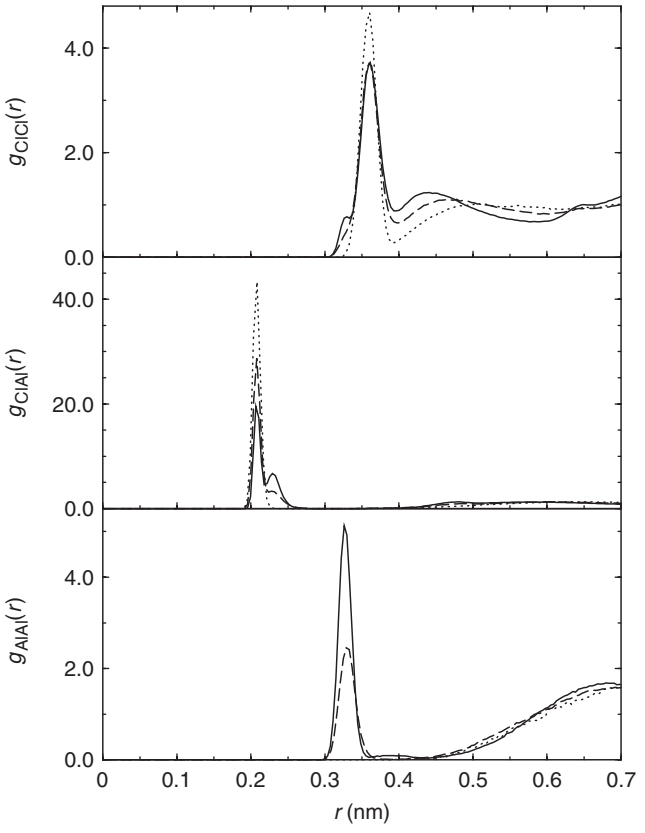

Figure 5. Illustrating the role of temperature in simulations of the partial pdfs in the $AlCl_3$ model taken at the equilibrium temperature-dependent density ρ (from data reported by Janz [30] extrapolated to 673 K). Full lines, $T = 473$ K and $\rho = 1.27\,\mathrm{g\,cm^{-3}}$; dashed lines, $T = 573$ K and $\rho = 1.0\,\mathrm{g\,cm^{-3}}$; dotted lines, $T = 673$ K and $\rho = 0.75\,\mathrm{g\,cm^{-3}}$.

(see also the discussion given below for the temperature dependence of $G(r)$). In this region the neutron diffraction data show only skewness in the first-neighbor peak. The above statements are quantified by reporting in table 1 the main bond lengths in liquid MCl_3 (with M = Al or Fe) from the present simulation models and from the neutron diffraction experiments [11,12], in comparison with those measured for the isolated molecular dimer by electron diffraction on the gas [31,32].

It is also evident from figure 3 that the sharpness of the pair-correlation peaks and the flatness of the trough are overemphasized in the simulation model. It should be stressed again at this point that the model evaluates the partial pdfs by direct counting of bond lengths, whereas the experiments obtain $G(r)$ by Fourier inversion of the neutron-weighted total structure factor $S(k)$. Quantitative faults may arise in the simulation model from various defects in the adjustment of its parameters to molecular data, such as the neglect of anharmonicity in molecular vibrations and of finite temperature effects, or the assumption of nominal ionic valences for the Coulomb interactions. On the other hand, the resolution of structures in $G(r)$ from Fourier inversion of $S(k)$ could be affected by truncation in momentum space. To examine this question we have evaluated $G(r)$ by Fourier inversion of $S(k)$ as obtained in the simulation model from

Table 1. Near-neighbor bond lengths in MCl_3 (in nm) from our simulation model of the liquid (SML), from neutron diffraction (NDL) and X-ray diffraction (XDL) experiments on the liquid, and from electron diffraction experiments on the gas (EDG).

	M–Cl^T	M–Cl^B	M–M	Cl^T–Cl^T	Cl^B–Cl^B
M = AI					
SML	0.207	0.228	0.327	0.360	0.329
NDL [11]	0.21	–	–	0.35	–
XDL [9]	0.206	0.234	0.328	0.365	0.328
EDG [31]	0.2065	0.2252	0.321	0.364	0.316
M = Fe					
SML	0.217	0.23	0.32	0.38	0.39
NDL + XDL [6]	0.22	–	–	0.37	–
EDG [32]	0.2127	0.2326	0.320	0.372	0.337

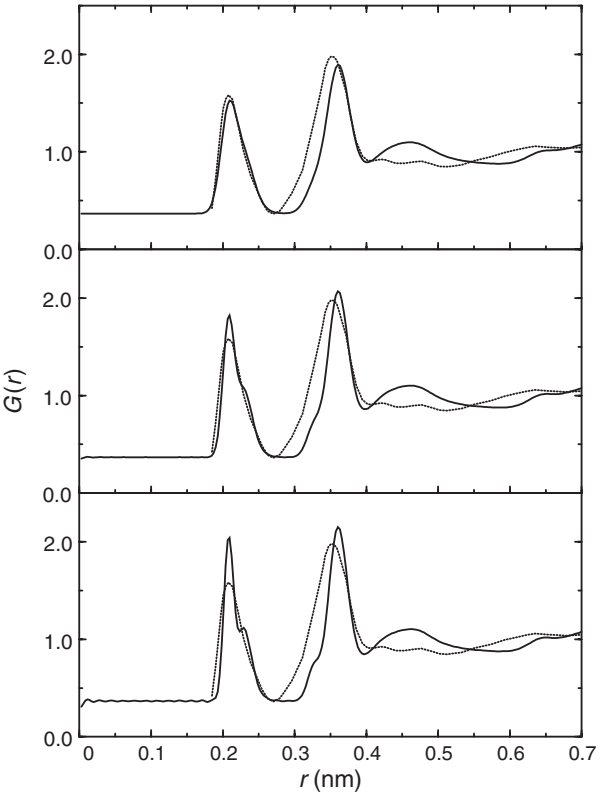

Figure 6. Illustrating the effect of varying a momentum cut-off in obtaining $G(r)$ by Fourier inversion of $S(k)$ in the present model for molten $AlCl_3$ (full lines: from top to bottom, $\sigma = 100$, 150, and 200 nm^{-1}). The dotted lines report the neutron diffraction data of Badyal *et al.* [11].

the correlations of density fluctuations, after windowing it with a factor $\exp[-q^2/(2\sigma^2)]$. The dashed lines in figure 3 show the result for the case $\sigma = 150\,nm^{-1}$, and figure 6 shows the dependence of the result on the value of σ for the case of $AlCl_3$ as a system-specific illustration of the challenge posed to neutron diffraction experiments on molecular liquids by the revelation of sharp local structures in **r**-space.

We turn next to discuss the results reported in figures 4 and 5. There evidently is in figure 4 at least semi-quantitative agreement between our classical simulation results based on interionic force laws and the *ab initio* simulation data based on quantum energy functionals. The following comments can be made with regard to quantitative details: (i) the *ab initio* simulation tends to overestimate the bond lengths by about 0.01 nm in comparison with the classical simulation and the neutron diffraction data; and (ii) the chlorine–chlorine correlations in the *ab initio* simulation show a broader first-neighbor peak and lack the broad hump located around 0.44 nm. We believe that the latter discrepancy signals differences in the intermediate range connectivity of the melt: the classical model as implemented in our simulations over-emphasizes to some extent the stability of dimeric states and tends to depress higher polymeric groups, whereas the *ab initio* calculations yield a more realistic balance between edge-sharing connectivity in the dimer and corner-sharing connectivity in higher polymers. In particular, Kirchner *et al.* [22] draw attention to corner-sharing in ring-shaped trimers, whereas in our classical simulations only occasionally during the evolution of the sample we can see formation of trimer-like states (usually in the form of a distorted monomer close to a terminal halogen in a dimer). We can also observe occasional formation of ionized states in the form of $M_2Cl_7^-$ groups.

It is evident from figure 5, on the other hand, that dimers (and presumably also higher polymers) in molten $AlCl_3$ are rapidly dissolving into monomers as the temperature of the simulation sample is raised. We have already cited in section 1 the experimental evidence for the dissolution of dimers into monomers in the gaseous phase. The dissociation process in our simulations of the liquid is well on its way at 573 K and is completed at 673 K, the revealing structural features being the decrease and ultimate disappearance of the peaks associated with the $Al–Cl^B$ and Al–Al correlations. This process is accompanied by enhancements of the $Al–Cl^T$ and Cl–Cl peaks, which can be understood as resulting from the strong decrease in density of a molecular liquid increasingly made from monomers. Our quantitative estimate is that the dimer/monomer concentration ratio changes from about 6 at 473 K to 0.44 at 573 K and to 0 at 673 K. These numbers are merely indicative, in view of the limited size of the sample.

3.3. *Angular distributions*

We complete the presentation of our results for the structure of a simulation model of molten $FeCl_3$ near freezing by reporting in figure 7 the distribution of angles subtended by various triplets of ions (very similar results are obtained for $AlCl_3$). There is a fairly close correspondence between these distributions and the structural angles in a rigid stick-and-ball model of the isolated molecular dimer, whose values are shown in figure 7 by arrows. Angular resolution has been enhanced in figure 7 by distinguishing with different types of arrows between triplets involving terminal or bridging chlorines (or both) in the isolated dimer, and by selecting different sets of bond lengths for the triplets in the model liquid. The area under each curve is proportional to the number of angles counted in correspondence to the maximum cutoff.

The two values of the cutoff that we have chosen for the Fe–Cl pairs correspond to including only the first part of the Fe–Cl peak in $G(r)$, up to the shoulder, or to including entirely the first-neighbor shell. Comparison of the corresponding angular

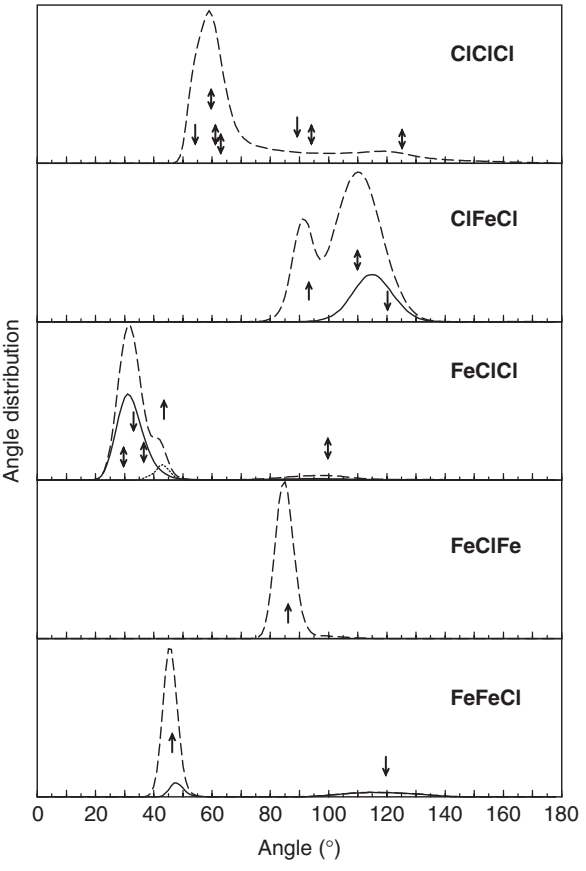

Figure 7. Distributions of angles subtended by various ion triplets in the simulation model of molten $FeCl_3$, for various cut-offs d_{AB} (nm) in the bond lengths of each triplet (full lines: $d_{Fe-Fe}=0.35$, $d_{Cl-Cl}=0.40$, $d_{Fe-Cl}=0.225$; dashed lines: $d_{Fe-Fe}=0.35$, $d_{Cl-Cl}=0.40$, $d_{Fe-Cl}=0.28$; dotted lines: $d_{Fe-Fe}=0.35$, $d_{Cl-Cl}=0.35$, $d_{Fe-Cl}=0.28$). The arrows show the location of ion-triplet angles in a rigid model of the isolated molecular dimer: downward arrows refer to bridging chlorines, upward arrows to terminal chlorines, and two-headed arrows to both.

distributions with the angles in the isolated dimer allows an unambiguous identification of two populations of chlorines in the first peak in $g_{Fe-Cl}(r)$: the terminal chlorines of the dimer correspond to the main peak, while the bridging chlorines are responsible for the shoulder.

3.4. *Single-particle motions and self-diffusion coefficients*

Finally, figure 8 reports our results for the msd of the ionic species in the two melts as functions of time. The corresponding values of the self-diffusion coefficients are obtained from the asymptotic slope of the msd (in units of $10^{-6}\,cm^2\,s^{-1}$) as $D_{Al}=2.32$ and $D_{Cl}=4.42$ in $AlCl_3$, $D_{Fe}=1.72$ and $D_{Cl}=2.65$ in $FeCl_3$. According to the discussion given in section 1 for ionic conductivity data and in section 3.2 for structural data, we expect that our model underestimates the value of D_{Cl} in $FeCl_3$. Of course,

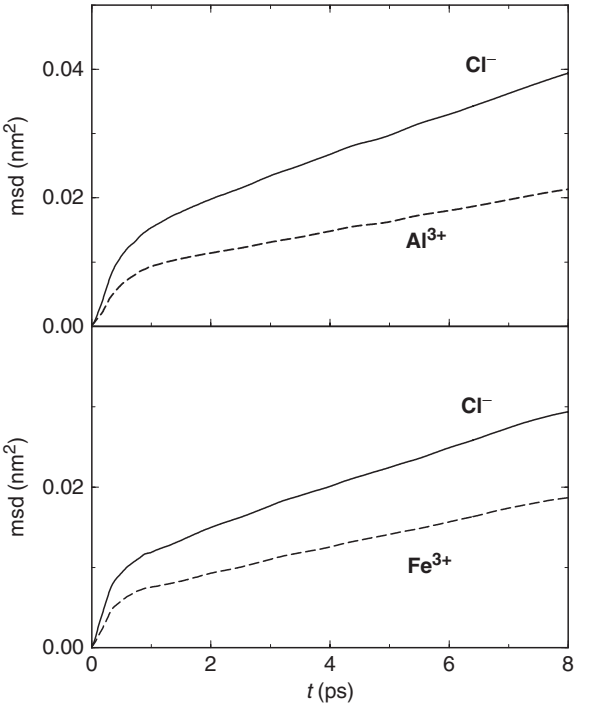

Figure 8. Mean square displacement (in nm^2) of the two ionic species in the present model for molten $AlCl_3$ (top) and molten $FeCl_3$ (bottom), as a function of time t (in ps).

it would be wholly inappropriate to estimate from these data the ionic conductivity in such mainly molecular liquids by means of the Nernst–Einstein relation. Diffusion is here mostly associated with translational and rotational motions of neutral molecular units, whereas ionic conduction requires ionization processes and hopping motions of halogen ions [14]. As already mentioned, we occasionally observe such ionization processes during the evolution of the simulation samples, but the statistics are much too low for any estimate of electrical transport.

4. Summary and future perspectives

In summary, the main focus of our work has been to give a comparative discussion of the results from molecular dynamics simulation and from neutron and X-ray diffraction experiments on the liquid structure of $AlCl_3$ and $FeCl_3$ melts. The simulation model has used interionic force laws strictly determined from properties of molecular dimers in the gaseous phase of these compounds, as described in terms of the interactions between the individual component ions. The model is seen to have some predictive value, which will be especially useful for the estimation of structural and transport properties on the approach to states that are expected to be met under extreme conditions of temperature and pressure, as the liquid structure is broken up into that of a dissociated ionic liquid. Model studies would allow rapid exploration of such transitions in the fluid state, to be ultimately examined by computer-expensive quantum simulation methods.

Our results provide some new evidence that (i) the liquid structure of molten $AlCl_3$ near freezing has stable Al_2Cl_6 molecular units as important constituents with strong intermolecular correlations; and (ii) the liquid structure of molten $FeCl_3$ near freezing deviates to some minor extent from a similar modelistic view involving Fe_2Cl_6 molecular units. The concentration of dimers relative to monomers and higher polymers is very sensitively dependent on temperature and on model parameters such as the ionic valences. The dimers in both melts appear to be very stable in our simulations runs, which yield almost completely dimerized samples near nominal freezing.

With regard to future developments, three main perspectives suggest themselves. Firstly, studies of the equation of state of these compounds in both the vapor and the liquid phase are called for. Secondly, improvements in the model may be sought with the help of liquid-state data: the best candidates in this respect are the width of the first-neighbor shell and the intermediate halogen–halogen correlations, which are expected to be very sensitive to the introduction of deviations from the nominal ionic valences. Thirdly, the study of transport in the liquid phase should be extended to other properties that would directly reflect the correlated motions of the two ionic species.

Acknowledgements

We are very grateful to Dr Barbara Kirchner for providing us with the results of the *ab initio* simulation runs published in [22]. One of us (Z. Akdeniz) acknowledges support from TUBITAK and from the Research Foundation of Istanbul University under Project Number UDP-786/23062006. Z.A. and M.P.T. thank Professor V.E. Kratsov and the Condensed Matter and Statistical Physics Section of the Abdus Salam International Center for Theoretical Physics in Trieste for their hospitality.

References

[1] M.P. Tosi, D.L. Price, M.-L. Saboungi. *Ann. Rev. Phys. Chem.*, **44**, 173 (1998).
[2] N.H. March, M.P. Tosi. *Phys. Chem. Liq.*, **10**, 39 (1980).
[3] G.N. Papatheodorou. *J. Chem. Phys.*, **66**, 2893 (1977).
[4] M.-L. Saboungi, D.L. Price, C. Scamehorn, M.P. Tosi. *Europhys. Lett.*, **15**, 283 (1991).
[5] M. Blander, E. Bierwagen, K.G. Calkins, L.A. Curtiss, D.L. Price, M.-L. Saboungi. *J. Chem. Phys.*, **97**, 2733 (1992).
[6] Y.S. Badyal, M.-L. Saboungi, D.L. Price, D.R. Haeffner, S.D. Shastri. *Europhys. Lett.*, **39**, 19 (1997).
[7] M.-L. Saboungi, M.A. Howe, D.L. Price. *Molec. Phys.*, **79**, 847 (1993).
[8] Z. Akdeniz, M.P. Tosi. *Proc. R. Soc. London*, **A437**, 85 (1992).
[9] R.L. Harris, R.E. Wood, H.L. Ritter. *J. Amer. Chem. Soc.*, **73**, 3150 (1951).
[10] A.D. Alvarenga, M.-L. Saboungi, L.A. Curtiss, M. Grimsditch, L.E. McNeil. *Molec. Phys.*, **81**, 409 (1994).
[11] Y.S. Badyal, D.A. Allen, R.A. Howe. *J. Phys.: Condens. Matter*, **6**, 10193 (1994).
[12] D.L. Price, M.-L. Saboungi, Y.S. Badyal, J. Wang, S.C. Moss, R.L. Leheny. *Phys. Rev.*, **B57**, 10496 (1998).
[13] H.A. Andreasen, N.J. Bjerrum, N.H. Hansen. *J. Chem. Eng. Data*, **25**, 236 (1980).
[14] Z. Akdeniz, M.P. Tosi. *Zs. Naturforsch.*, **53a**, 960 (1998).
[15] L. Nalbandian, G.N. Papatheodorou. *High Temp. Sci.*, **28**, 49 (1994).
[16] M. Blander. *Molten Salt Chemistry*, Interscience, New York (1964).
[17] K. Aarset, Q. Shen, H. Thomassen, A.D. Richardson, K. Hedberg. *J. Phys. Chem. A*, **103**, 1644 (1999).
[18] Z. Akdeniz, G. Pastore, M.P. Tosi. *N. Cimento*, **20D**, 595 (1998).
[19] M.C. Abramo, C. Caccamo. *J. Phys. Condens. Matter*, **6**, 4405 (1994).

[20] F. Hutchinson, M.K. Walters, A.J. Rowley, P.A. Madden. *J. Chem. Phys*., **110**, 5821 (1999).
[21] F. Hutchinson, M. Wilson, P.A. Madden. *Molec. Phys*., **99**, 811 (2001).
[22] B. Kirchner, A.P. Seitsonen, J. Hutter. *J. Phys. Chem. B*, **110**, 11475 (2006).
[23] A. Karaman, Z. Akdeniz, M.P. Tosi. *Phys. Chem. Liq*., **44**, 353 (2006).
[24] G. Pastore, Z. Akdeniz, M.P. Tosi. *J. Phys.: Condens. Matter*, **3**, 8297 (1991).
[25] Z. Akdeniz, R. Ruberto, G. Pastore, M.P. Tosi. *Proc. XV Int. Symp. Molten Salts, ECS Transactions* (In press).
[26] W.R. Busing. *Trans. Am. Crystallogr. Ass*., **6**, 57 (1970).
[27] A.R. Cochran. *Crit. Rev. Solid State Sci*., **2**, 1 (1971).
[28] Z. Akdeniz, M.P. Tosi. *Zs. Naturforsch*., **54a**, 180 (1999).
[29] M.P. Allen, D.J. Tildesley. *Computer Simulation of Liquids*, Oxford University Press, New York (1987).
[30] G.J. Janz. *J. Phys. Chem. Ref. Data*, **17**, 1795 (1988).
[31] M.W. Chase, C.A. Davies, J.R. Downey, D.J. Frurip, R.A. McDonald, A.N. Syverud. *J. Phys. Chem. Ref. Data*, **14**, 1 (1985).
[32] M. Hargittai, J. Tremmel, I. Hargittai. *J. Chem. Dalton Trans*., **1**, 87 (1980).